



Article

Enhanced Visible Light-Driven Photoelectrocatalytic Degradation of Paracetamol at a Ternary z-Scheme Heterojunction of Bi₂WO₆ with Carbon Nanoparticles and TiO₂ Nanotube Arrays Electrode

Nondumiso Mahhumane ^{1,2}, Leskey M. Cele ^{1,*}, Charles Muzenda ², Oluchi V. Nkwachukwu ², Babatunde A. Koiki ² and Omotayo A. Arotiba ^{2,3,*}

¹ Department of Chemistry, Tshwane University of Technology, Pretoria 0001, South Africa; nondumiso.mahhumane@gmail.com

² Department of Chemical Sciences, University of Johannesburg, Johannesburg 2028, South Africa; simbacharlee@gmail.com (C.M.); oluviv2000@yahoo.com (O.V.N.); bakoiki@gmail.com (B.A.K.)

³ Centre for Nanomaterials Science Research, University of Johannesburg, Johannesburg 2028, South Africa

* Correspondence: celelm@tut.ac.za (L.M.C.); oarotiba@uj.ac.za (O.A.A.)



Citation: Mahhumane, N.; Cele, L.M.; Muzenda, C.; Nkwachukwu, O.V.; Koiki, B.A.; Arotiba, O.A. Enhanced Visible Light-Driven Photoelectrocatalytic Degradation of Paracetamol at a Ternary z-Scheme Heterojunction of Bi₂WO₆ with Carbon Nanoparticles and TiO₂ Nanotube Arrays Electrode. *Nanomaterials* **2022**, *12*, 2467. <https://doi.org/10.3390/nano12142467>

Academic Editors: Hermenegildo García and Amarajothi Dhakshinamoorthy

Received: 3 June 2022

Accepted: 4 July 2022

Published: 19 July 2022

Publisher's Note: MDPI stays neutral with regard to jurisdictional claims in published maps and institutional affiliations.



Copyright: © 2022 by the authors. Licensee MDPI, Basel, Switzerland. This article is an open access article distributed under the terms and conditions of the Creative Commons Attribution (CC BY) license (<https://creativecommons.org/licenses/by/4.0/>).

Abstract: In this study, a ternary z-scheme heterojunction of Bi₂WO₆ with carbon nanoparticles and TiO₂ nanotube arrays was used to remove paracetamol from water by photoelectrocatalysis. The materials and z-scheme electrode were characterised using X-ray diffraction (XRD), field emission scanning electron microscopy (FESEM), energy dispersive X-ray spectroscopy (EDS), EDS mapping, ultraviolet diffuse reflection spectroscopy (UV-DRS), photocurrent measurement, electrochemical impedance spectroscopy (EIS), uv-vis spectroscopy and total organic carbon measurement (TOC). The effect of parameters such as current density and pH were studied. At optimal conditions, the electrode was applied for photoelectrocatalytic degradation of paracetamol, which gave a degradation efficiency of 84% within 180 min. The total organic carbon removal percentage obtained when using this electrode was 72%. Scavenger studies revealed that the holes played a crucial role during the photoelectrocatalytic degradation of paracetamol. The electrode showed high stability and reusability therefore suggesting that the z-scheme Bi₂WO₆-CNP-TiO₂ nanotube arrays electrode is an efficient photoanode for the degradation of pharmaceuticals in wastewater.

Keywords: photoelectrocatalytic degradation; paracetamol; z-scheme heterojunction; bismuth tungstate; carbon nanoparticle; titania nanotube array; water treatment

1. Introduction

Paracetamol, also known as acetaminophen, is one of the most prescribed drugs used for the treatment of pain, aches and fevers [1–4]. The discharge of paracetamol into aqueous environment can reach a toxic level that is harmful to humans and aquatic life [5]. Paracetamol reaches water bodies through the disposal of effluents, discharge of faeces/urine or through hospital sewage [6]. Due to the difficulty in the removal of paracetamol from water during treatment, advanced oxidation processes have been used for its removal in water instead of conventional methods [1,7]. Photo-fenton, sonolysis and H₂O₂/UV are extensively used advanced oxidation processes for the removal of paracetamol in water and wastewater [8,9]. Amongst other different types of AOPs, photoelectrocatalysis is gaining popularity due to its simplicity, low maintenance, positive environmental impact, recycling and reusability [10]. This method involves the use of a semiconductor immobilized on an electrochemical substrate [11–13]. Researchers have reported several different photoelectrocatalytic systems including single semiconductor systems. The problem with the single semiconductor systems for the degradation of paracetamol is that it cannot possess wide absorption and strong redox abilities simultaneously [14,15]. For instance, Bi₂WO₆ is a

single semiconductor that has been used in the PEC degradation of organic pollutants [16]. Bi_2WO_6 is a typical Aurivillius oxide with a perovskite layered structure and a high surface area, which means it has sufficient active sites to promote photocatalysis [14,16]. Bi_2WO_6 also has a narrow band gap of 2.7 eV, which means it has strong light harvesting ability compared to TiO_2 . However, Bi_2WO_6 is limited by its low separation efficiency and its inability to fully utilize solar energy [15]. To overcome the challenge of low separation efficiency and improve the photocatalytic potency of Bi_2WO_6 (and most semiconductors in general), z-scheme photoanodes have been constructed via two semiconductors of dissimilar/similar band gap and one electron mediator or conductor. This system mimics the photosynthesis process which includes a two-step photoexcitation [14,15,17]. In a typical mechanism, electrons of photocatalyst I are recombined with holes in photocatalyst II via an electron mediator under light. This process inhibits the recombination of photo-induced charge carriers while they keep their redox properties [14,15,17,18].

In this study, bismuth tungstate and anodised TiO_2 serve as photocatalyst I and II, respectively. TiO_2 is the most widely studied semiconductor with properties such as low toxicity, cost effectiveness and excellent stability [19–21]. In recent years, researchers have synthesized a unique morphology of highly ordered TiO_2 nanotube arrays (NTA). TiO_2 NTA consists of a high surface area and unique cylindrical structure with improved electron transport efficiency compared to common TiO_2 nanoparticles [22]. Amongst other different synthetic routes, anodisation of Ti sheets has been widely used, as it tends to give rise to a well-aligned structure with tuneable morphology and inner diameter. Anodised TiO_2 are cost effective and provide better reusability compared to powdered TiO_2 photocatalysts as they tend to disperse in solution during a reaction [22]. Unfortunately, TiO_2 NTA only needs UV light for activation due to its wide band gap [22]. The formation of the z-scheme heterojunction with a narrow band gap semiconductor such as Bi_2WO_6 , will solve this problem by tuning TiO_2 NTA towards solar activation. To improve the conductivity of Bi_2WO_6 and TiO_2 NTA, carbon nanoparticles (CNP) were used as an electron mediator. Nanomaterials have been incorporated into semiconductor structures as dopants or heterostructures for the enhancement of electrochemical, photocatalytic or photoelectrocatalytic properties, especially in the visible light [13,23,24].

Bi_2WO_6 has been applied in the photocatalytic degradation of organic pollutants and some of these reports used the z-scheme heterojunction approach. For example, Sharma et al. used a z-scheme of Bi_2WO_6 and titania for the degradation of antibiotics [14]. Hu et al. added porphyrin to Bi_2WO_6 for a z-scheme for photocatalytic application [15]. A recent review by Khedr et al. [25] highlights various photocatalytic applications of Bi_2WO_6 . To the best of our knowledge, our work presents the photoelectrocatalytic application of a Bi_2WO_6 based photoanode for the first time. While TiO_2 powder has been composited with Bi_2WO_6 , this report used a novel route of anodized titanium sheet to form TiO_2 NTA as a support for Bi_2WO_6 in the design of the z-scheme photoanode. The challenge of catalyst recovery, usually experienced in photocatalysis, is mitigated by the immobilization of the semiconductor on an electrode (photoanode) in photoelectrocatalysis, as in this case [10,26].

Bi_2WO_6 was coupled with CNP forming a $\text{Bi}_2\text{WO}_6/\text{CNP}$ nanocomposite. The resulting $\text{Bi}_2\text{WO}_6/\text{CNP}$ nanocomposite was immobilized on the surface of TiO_2 NTA, giving rise to a novel ternary z-scheme photoelectrocatalyst ($\text{Bi}_2\text{WO}_6/\text{CNP}/\text{TiO}_2$ NTA) for the degradation of paracetamol under visible light. The extent of degradation was monitored by uv/vis spectroscopy and total organic carbon measurements.

2. Materials and Methods

2.1. Chemicals

Bismuth (III) nitrate pentahydrate, sodium tungsten oxide dehydrate, acetone, ethanol, nitric acid, orthophosphoric acid, ammonium fluoride and glucose were purchased from Sigma Aldrich, Johannesburg, South Africa and were used as received. All reagents were in analytical grade and were used without further purification.

2.2. Preparation of z-Scheme $\text{Bi}_2\text{WO}_6/\text{CNP}/\text{TiO}_2$ NTA

Firstly, Bi_2WO_6 was synthesized by Sharma et al.'s 2020 method with slight modification, using the solvothermal method. A mass of 1.455 g of bismuth nitrate pentahydrate ($\text{Bi}(\text{NO}_3)_3 \cdot 5\text{H}_2\text{O}$) was solubilized in 37.5 mL of ethylene glycol, instead of deionized water, and labelled as solution A. Next, 0.5 g of sodium tungstate dehydrate ($\text{Na}_2(\text{WO}_4) \cdot 2\text{H}_2\text{O}$) was dissolved in 12.5 mL of ethylene glycol and labelled as solution B. Solution B was introduced to solution A under sonication with dropwise addition. The resulting solution was stirred for an hour and then transferred into an autoclave for solvothermal treatment at 160 °C for 25 h. After the reaction, a brown precipitate was collected via centrifugation, washed with ethanol and water thoroughly and dried at 50 °C overnight.

The Bi_2WO_6 -CNP composite was prepared by the dispersion of synthesized Bi_2WO_6 in absolute ethanol and sonicated for 50 min to obtain uniformity of suspension of the particles followed by the addition of 10 to 30% weight of the previously prepared CNP, using a method suggested by Tshwenya and Arotiba [27]. The mixture was further sonicated for 30 min. The mixture was placed in the oven to dry at 100 °C overnight for the complete evaporation of ethanol. The resulting composite was placed in the muffle furnace for 2 h at 500 °C.

A highly ordered TiO_2 NTA was prepared using the approach reported by Koiki et al. [22]. Titanium sheets of 5 × 3 cm were used as the substrate for the fabrication of TiO_2 NTA. Before the anodisation process, the sheets were sonicated in detergents acetone, ethanol, nitric acid and deionised water, respectively, and dried in the oven. The anodisation process was performed with a two-electrode electrochemical cell connected to a DC power source. A platinum foil was used as a counter electrode and was placed at a 2 cm distance from the titanium sheet anode. A potential of 25 V was applied to the electrochemical cell, which contained a mixture of 0.2 M H_3PO_4 and 0.3 M NH_4F as the electrolyte for 2 h while being stirred magnetically. Thereafter, the prepared electrode was rinsed with deionised water to eliminate blocked ions from its surface and subsequently annealed for 2 h with a heating and cooling rate of 10 °C/min. The Bi_2WO_6 -CNP composite was immobilized on the anodized TiO_2 NTA via a simple deposition where 10% wt of nafion was used as a binder. The electrode was then placed in the oven and left to dry overnight.

2.3. Characterisation

The crystalline properties of the fabricated powders were measured by X-ray diffraction (XRD, D8 Advance, Bruker, Germany). The morphology and structure were observed by scanning electron microscopy (SEM, Supra55, Zeiss, Germany) and transmission electron microscopy (TEM, JEM-2100, JEOL, Tokyo, Japan), and the element constitution was detected by energy-disperse X-ray spectroscopy (EDS). The Brunauer–Emmett–Teller (BET) surface areas of the as-prepared materials were measured using a surface area and porosity analyzer (Quadrasorb EVO, Quantachrome, Florida, USA) by nitrogen adsorption-desorption. The optical properties of various photocatalysts were examined by UV–Vis diffuse reflectance spectra (UV–Vis DRS, UH4150, Hitachi, Japan).

2.4. Electrochemical and Photoelectrochemical Characterisation

The electrochemical and photoelectrical measurements was conducted on Autolab PGSTAT204 (Barendrecht, Netherland) potentiostat/galvonstat with a three-electrode configuration. The fabricated electrode, platinum foil and Ag/AgCl (3.0 M KCl) were used as working electrodes, counter electrode and reference electrode, respectively. An Oriel LCS-100 W solar simulator with UV cut-off (λ less than 400 nm) was used as the light source for PEC experiment. The prepared electrode was positioned vertically facing the incident light of the simulator and the distance between the photoelectrochemical cell and the light source was kept constant at 10 cm. Photocurrent measurements and linear sweep voltammetry was carried out in a 0.1 M Na_2SO_4 solution. Cyclic voltammetry was carried out in a 5 mM solution of $[\text{Fe}(\text{CN})_6]^{3-/4-}$ (prepared in a 0.1 M KCl). For the degradation experiments, paracetamol solutions were prepared in 0.1 M Na_2SO_4 supporting electrode.

Electrochemical degradation experiments were carried out in the dark. An aliquot of the solution was collected from the reactor at certain time intervals using a disposal syringe. The concentration decay and degradation pattern of the analyte was observed using UV-visible spectrophotometer and the total organic removal was recorded using TOC. The effects of applied potential on the removal efficiency were investigated.

Figure 1 presents the schematics of the photoanode and the photoelectrochemical set-up for the degradation of paracetamol.

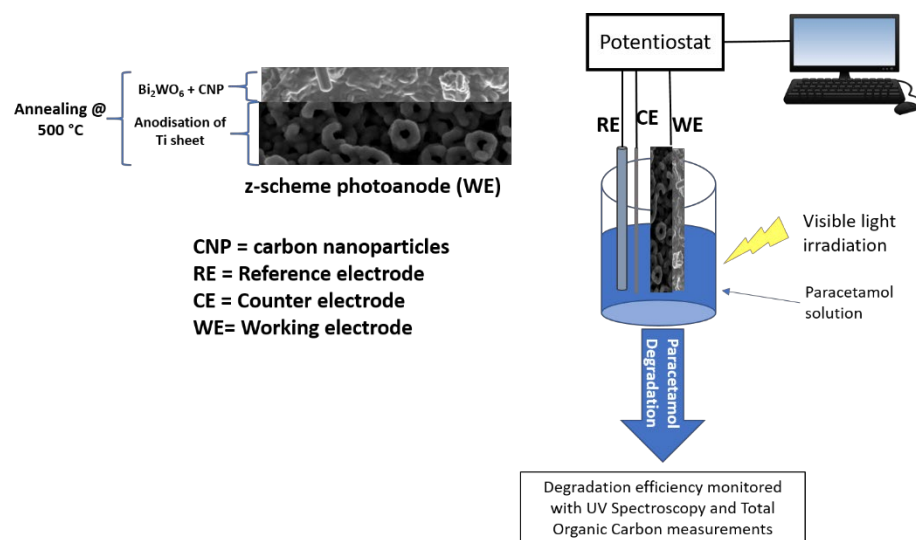


Figure 1. Schematic diagram of prepared $\text{Bi}_2\text{WO}_6\text{-CNP-TiO}_2$ NTA z-scheme photoanode used for photoelectrocatalytic degradation of paracetamol in a three-electrode cell.

3. Results

3.1. Structural and Morphological Characterisation

The crystal structure of the synthesized Bi_2WO_6 and $\text{Bi}_2\text{WO}_6\text{-CNP}$ composite was characterised by XRD as indicated in Figure 2a. The Bi_2WO_6 diffraction peaks at $2\theta = 28.34^\circ, 32.88^\circ, 47.06^\circ, 55.99^\circ, 58.59^\circ, 68.92^\circ, 75.97^\circ$ and 78.33° are attributed to the orthorhombic phase of the Bi_2WO_6 and are in agreement with JCPDS card no. 39-0256 (Sharma et al., 2020). However, after the addition of CNP on the surface of Bi_2WO_6 , new diffraction peaks were observed. The sharpest peak found at 28.7° may be an influence of highly disordered carbon atoms with amorphous nature, as seen in most carbon materials. Figure 2b presents the crystal structure of synthesized TiO_2 NTA and $\text{Bi}_2\text{WO}_6\text{-CNP-TiO}_2$ NTA. During the synthesis of TiO_2 NTA, it is important to control parameters such as the composition of the electrolyte, anodization potential and annealing temperature to achieve highly ordered tubes [22]. For instance, the use of a viscous electrolyte may lead to an excessive supply of oxygen ions than needed for oxidation [22]. The use of ethylene glycol may provide a slow anodic oxidation process and formation of glycolaldehyde and glycolic acid, making the donation of oxygen challenging [22]. Hence, the use of H_3PO_4 is advantageous, since it serves as a buffer and prevents rapid etching during nanotube growth [22]. Accurate anodization potential must be used, as high potential can damage the surface structure, resulting in disordered spongy porous tubes. The annealing temperature is also important as it gives rise to anatase and rutile form. At temperatures higher than 500°C , the anatase and rutile form begins to combine and at 800°C , they completely disappear [22]. As seen in Figure 2b the synthesized TiO_2 NTA shows diffraction peaks at $2\theta = 35.1^\circ, 38.4^\circ, 40.2^\circ, 53^\circ, 70.6^\circ$ and 76.2° , corresponding to (100), (002), (101), (102), (103) and (112) diffraction plane of Ti metal, respectively, and are in agreement with JCPDS card no. 04-004-7631. The TiO_2 NTA only showed anatase peaks at $2\theta = 25.3^\circ, 48.1^\circ, 62.7^\circ, \text{ and } 75.1^\circ$, corresponding to (101), (200), (204) and (205) in agreement with JCPDS card no 01-075-2546. This suggested that pure TiO_2 anatase was formed. After the deposition of $\text{Bi}_2\text{WO}_6\text{-CNP}$ on the surface of TiO_2 ,

the peaks belonging to Bi_2WO_6 -CNP and TiO_2 NTA were observed on the XRD pattern of Bi_2WO_6 -CNP- TiO_2 NTA, confirming the successful synthesis of the ternary composite. The crystallite size of Bi_2WO_6 and Bi_2WO_6 -CNP was calculated from Debye-Scherrer's formula, given by

$$D = 0.94 \lambda / \beta \cos \theta$$

where D is the average crystallite size, λ is the wavelength of X-ray radiation, β is the broadening of the diffraction line assessed at full width half maximum value (FWHM) and θ is the Bragg's angle. The crystallite size of Bi_2WO_6 and Bi_2WO_6 -CNP are 9.36 nm and 5.32 nm, respectively. The decrease in crystallite size shows that the Bi_2WO_6 -CNP has an increased surface area than the pure Bi_2WO_6 . BET analysis was carried out to further confirm the increase in surface area where Bi_2WO_6 gave a surface area of $6.3214 \text{ m}^2/\text{g}$ and Bi_2WO_6 -CNP gave a surface area of $15.0235 \text{ m}^2 \text{ g}^{-1}$.

The surface morphology of the prepared Bi_2WO_6 , Bi_2WO_6 -CNP, TiO_2 NTA and Bi_2WO_6 -CNP- TiO_2 NTA was investigated using FESEM, as seen in Figure 2c–f. The pure Bi_2WO_6 shows spherical aggregate morphology (Figure 2c). However, with Bi_2WO_6 -CNP the morphology of the aggregate changed to rod-like structures, as seen in Figure 2d. Figure 2e shows pristine TiO_2 NTA with highly ordered and well-oriented tubes, with an estimated diameter of 98 nm and wall thickness of 18 nm around them. After deposition, the agglomerated rod-like structures of Bi_2WO_6 -CNP cover the surface of the TiO_2 NTA as seen in Figure 2f. However, the TiO_2 holes can be seen within the Bi_2WO_6 -CNP, indicating that both materials are present on the electrode. The EDS spectrum in Figure 2g further confirms the elemental composition of Bi_2WO_6 -CNP- TiO_2 NTA with the following elements present in different proportions and quantities: Bi, Ti, W, C, and O. Other elements seen on the spectrum are due to the binder used for deposition. The EDS mapping analysis in Figure 2h validates the existence and even distribution of the elements Bi, Ti, W, C, and O, making up the Bi_2WO_6 -CNP- TiO_2 NTA electrode.

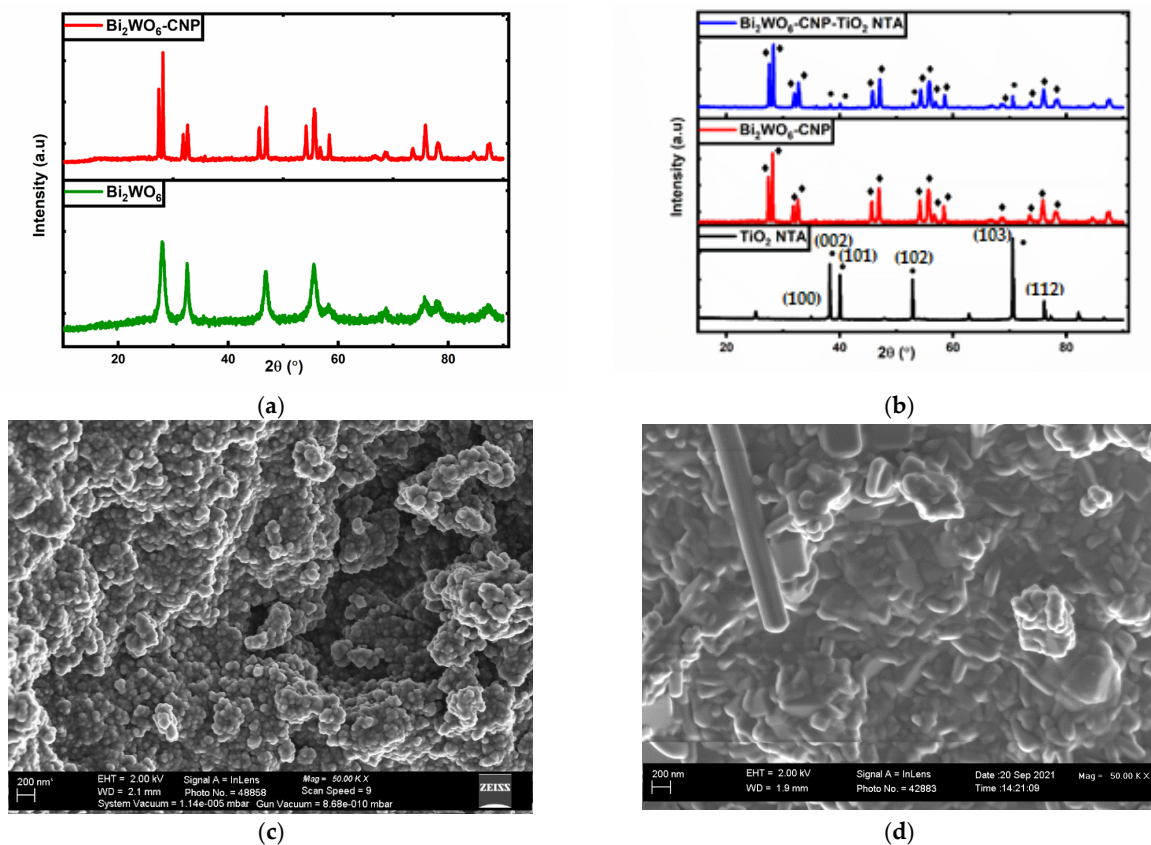
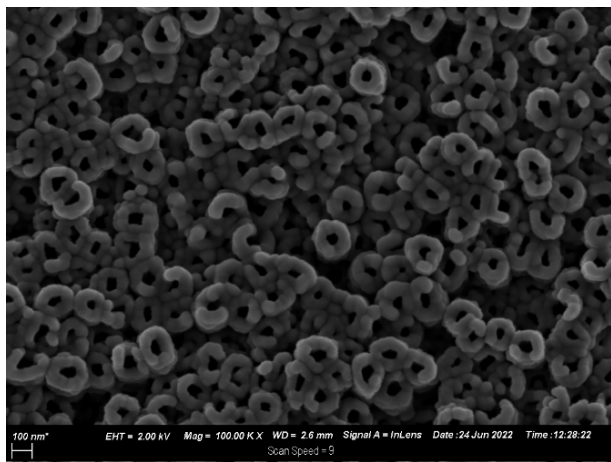
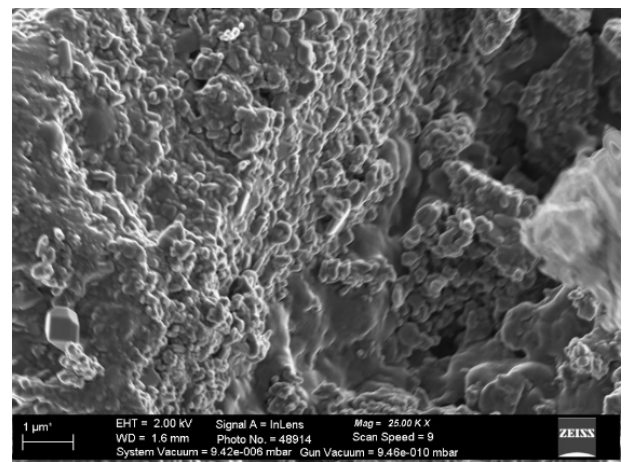


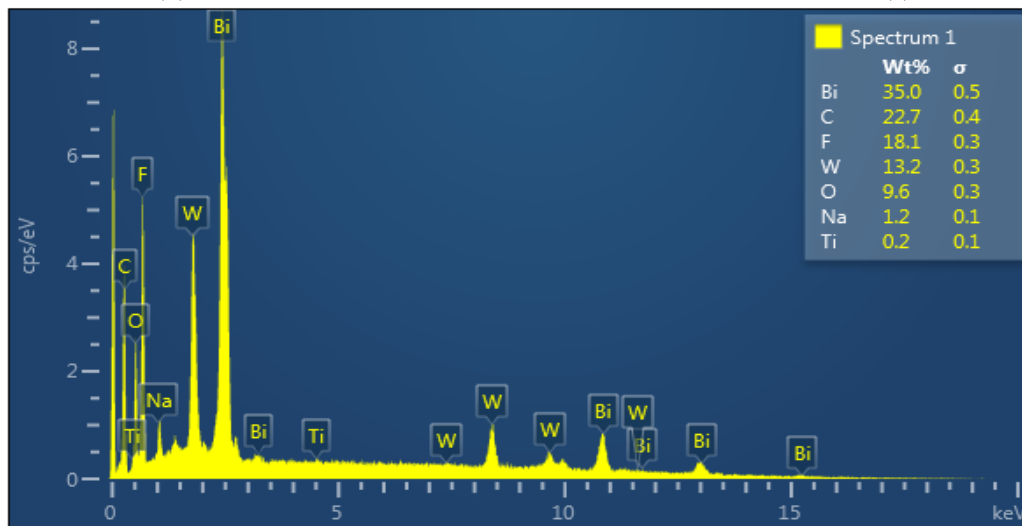
Figure 2. Cont.



(e)



(f)



(g)

EDS Layered Image 1



Figure 2. Cont.

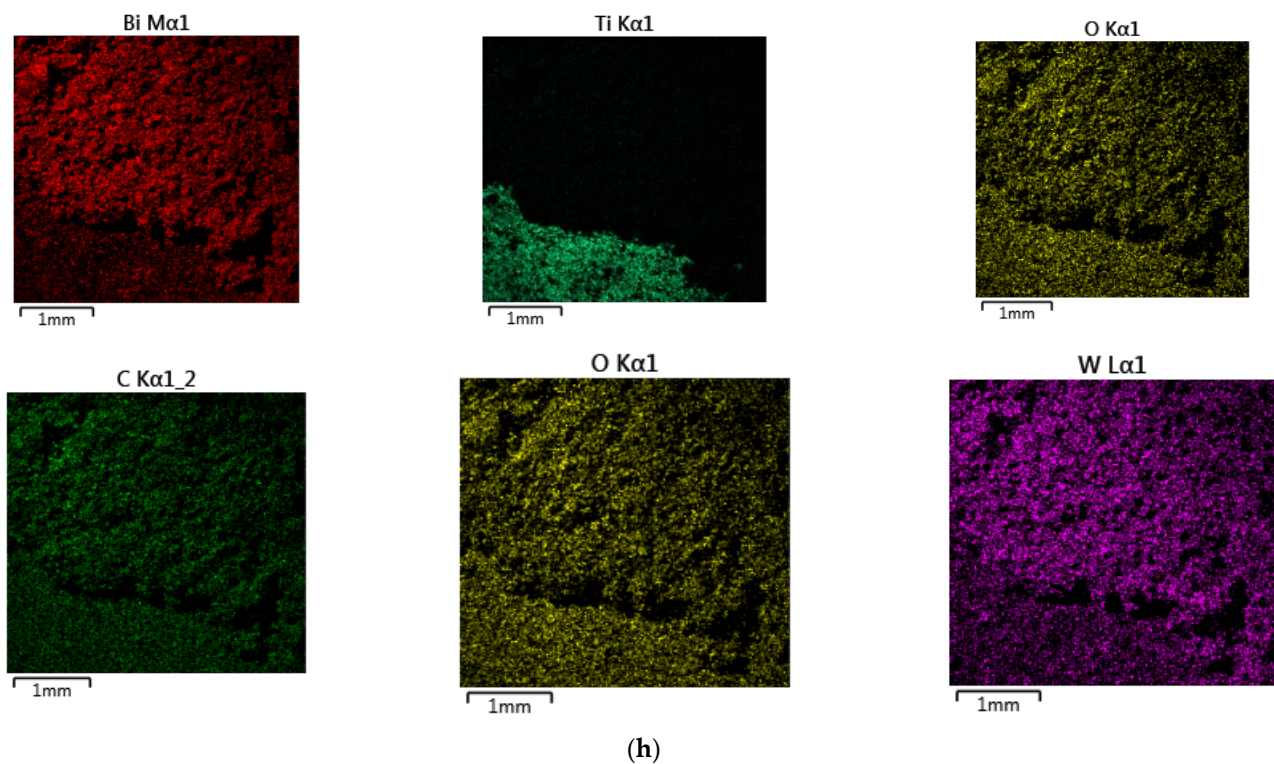


Figure 2. XRD patterns of (a) Bi_2WO_6 and Bi_2WO_6 -CNP, (b) TiO_2 NTA and Bi_2WO_6 -CNP- TiO_2 NTA. FESEM images of (c) Bi_2WO_6 ; (d) Bi_2WO_6 -CNP; (e) TiO_2 NTA; (f) Bi_2WO_6 -CNP- TiO_2 NTA; (g) EDS spectrum of Bi_2WO_6 -CNP- TiO_2 NTA and (h) EDS elemental mapping of Bi_2WO_6 -CNP- TiO_2 NTA electrode.

3.2. Optical Properties

UV-vis diffuse reflectance spectroscopy shows that the Bi_2WO_6 -CNP- TiO_2 NTA electrode has higher absorbance than the TiO_2 -NTA electrode in the visible region of 400 to 800 nm (Figure 3a). This suggests that the formation of the z-scheme heterojunction has enhanced visible light activity.

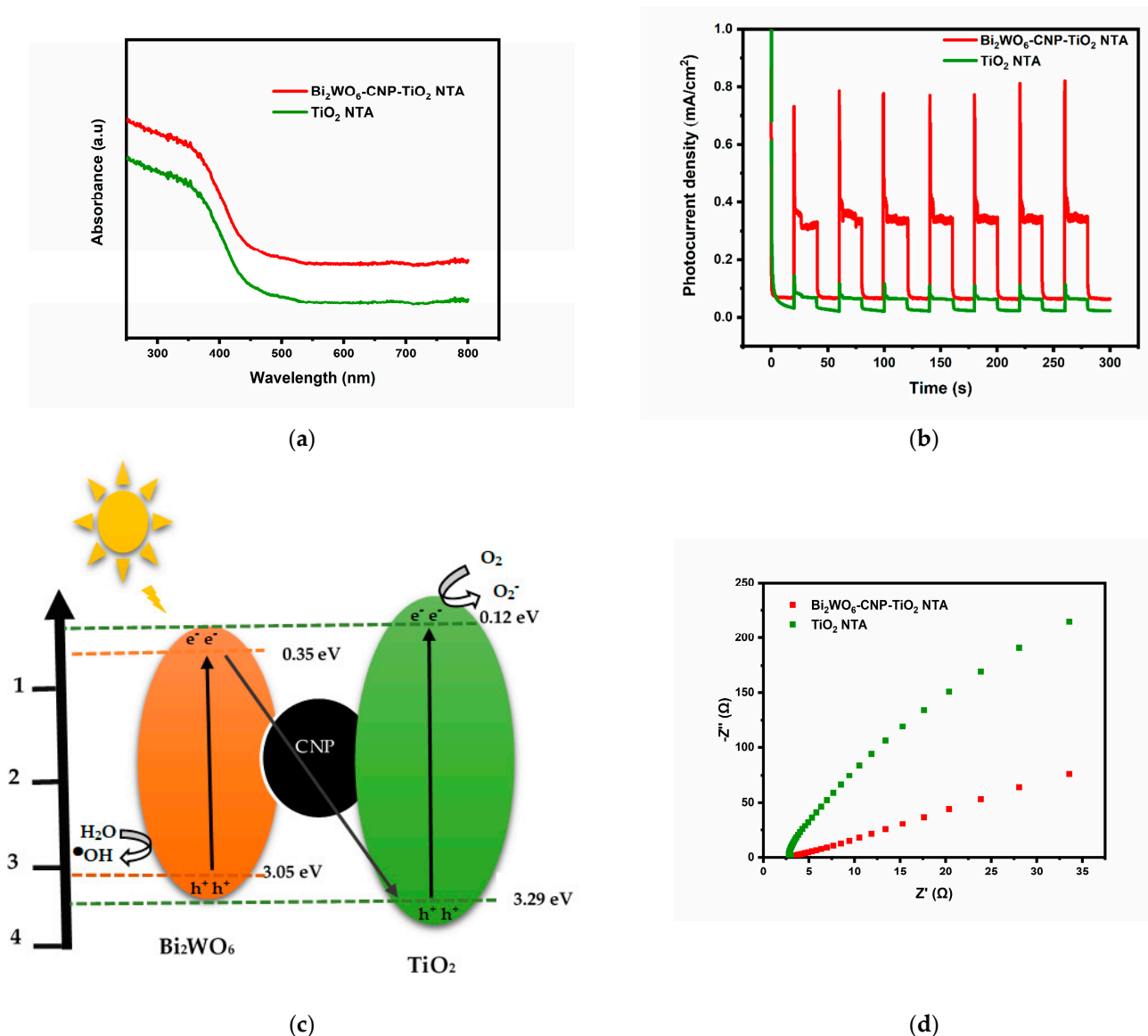


Figure 3. (a) UV-Visible diffuse reflectance spectra TiO₂ NTA Bi₂WO₆-CNP- TiO₂ NTA (b) photocurrent responses of TiO₂ NTA and Bi₂WO₆-CNP- TiO₂ NTA in 0.1 M Na₂SO₄ (c) schematic diagram of Z-scheme mechanism of Bi₂WO₆-CNP-TiO₂ NTA electrode (d) Nyquist plot TiO₂ NTA and Bi₂WO₆-CNP- TiO₂ NTA photoanodes in 5 mM [Fe(CN)₆]^{3-/4-} in 0.1 M KCl (pH 7).

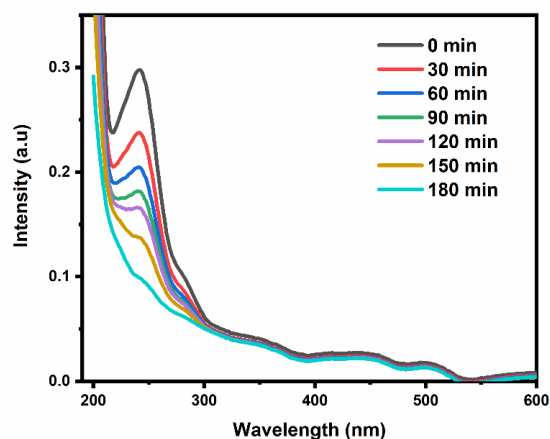
3.3. Electrochemical Studies

Figure 3b shows the chronoamperographs of pristine TiO₂ NTA and Bi₂WO₆-CNP-TiO₂ NTA under solar light illumination at 2 V bias potential using 0.1 M KCl solution. The two electrodes showed photocurrent responses (improved current in the presence of light than in the dark). However, the Bi₂WO₆-CNP-TiO₂ NTA electrode exhibits a more marked photocurrent response with a higher current density of 0.789 mA cm⁻² when compared to bare TiO₂ NTA with a current density of 0.172 mA cm⁻². The photocurrent density of Bi₂WO₆-CNP- TiO₂ NTA is about 4.6 times higher than the TiO₂ NTA. The increase could result from the z-scheme of heterojunction between Bi₂WO₆, CNP and TiO₂ NTA, giving rise to an improved separation of electron hole pairs (Figure 3c). To further confirm the improved performance of the prepared electrodes an experiment was conducted using electrochemical impedance spectroscopy. The experiment was performed in an electrolytic solution of 5 mM [Fe(CN)₆]^{3-/4-} in 0.1 M KCl at pH 7 with external application of +0.2 V. Figure 3d shows the Nyquist plot of the fabricated photoanodes

consisting of a semicircle, which represents the charge transfer process happening at the solution-electrode interface. The diameter of the semicircle represents the charge transfer resistance (R_{ct}) at the interface of the electrode. Lower R_{ct} values indicate a better charge transfer efficiency. The R_{ct} of TiO_2 NTA and $\text{Bi}_2\text{WO}_6\text{-CNP-TiO}_2$ NTA are 92.14Ω and 31.32Ω , respectively. This suggested that the fabrication of the z-scheme heterojunction has improved the charge mobility of the electrode and lowered the rate of instantaneous recombination of electron-hole pairs [11].

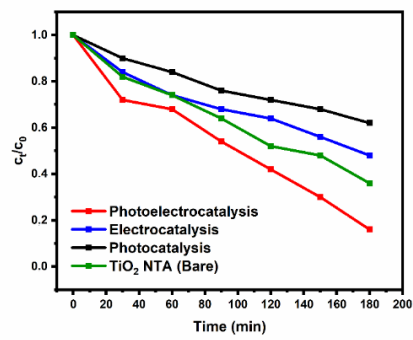
3.4. Photoelectrochemical Studies

The photoelectrocatalytic performance of the prepared electrodes was evaluated by applying it in a solar reactor for the degradation of paracetamol with an initial concentration of 5 mg L^{-1} . The degradation was accomplished with an applied current of 10 mA cm^{-2} , pH 7 and irradiation with solar light. UV-visible spectrophotometry was used to monitor the degradation efficiency of the electrode at a wavelength of 243.0 nm . Figure 4a shows the decrease in the intensity of the peak at 243.0 nm as the reaction time increases, representing the reduction in the concentration of the pharmaceutical. A degradation efficiency of 84% was achieved after 3 h when using the z-scheme electrode for photoelectrocatalysis, as presented in Figure 4b. When the $\text{Bi}_2\text{WO}_6\text{-CNP-TiO}_2$ NTA photoanode was applied for electrochemical oxidation of the paracetamol (that is without the stimulation of solar light), the degradation efficiency decreased to 57% (Figure 4b). In photocatalysis, where only the solar light was applied, a 42% degradation efficiency was recorded (Figure 4b). Photoelectrocatalytic (PEC) degradation of the paracetamol at the TiO_2 NTA only (that is without Bi_2WO_6) yielded 62%. These degradation percentages show that the formation of a z-scheme enhanced the PEC process. The degradation of paracetamol using the z-scheme electrode was further confirmed by the percentage of total organic carbon removal (TOC) which was 72, 30 and 22% for PEC, electrochemical oxidation (EC) and photocatalysis (PC), respectively. EC is the same setup as PEC but without irradiation with visible light, while PC is without the application of potential. This observation confirms that the synergy between solar energy and applied bias potential is crucial for breaking down the organic pollutant. Consequently, the solar energy promotes the generation of electron-hole pairs on the surface of the electrode, while the biased potential helps with the transfer of photo-excited electrons, which reduces the recombination of electron-hole pairs.

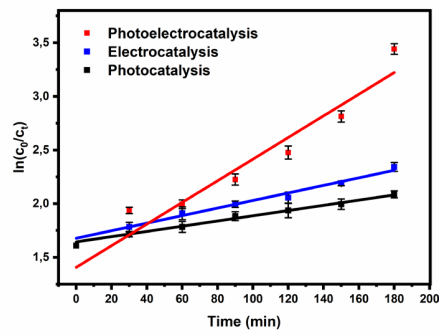


(a)

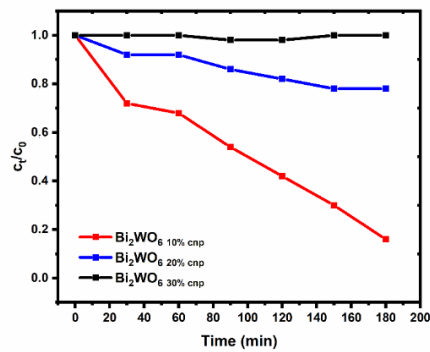
Figure 4. Cont.



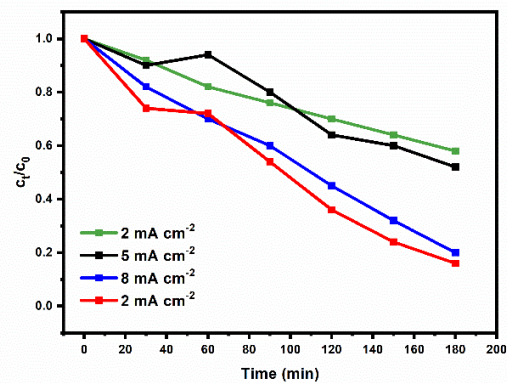
(b)



(c)



(d)



(e)

Figure 4. Cont.

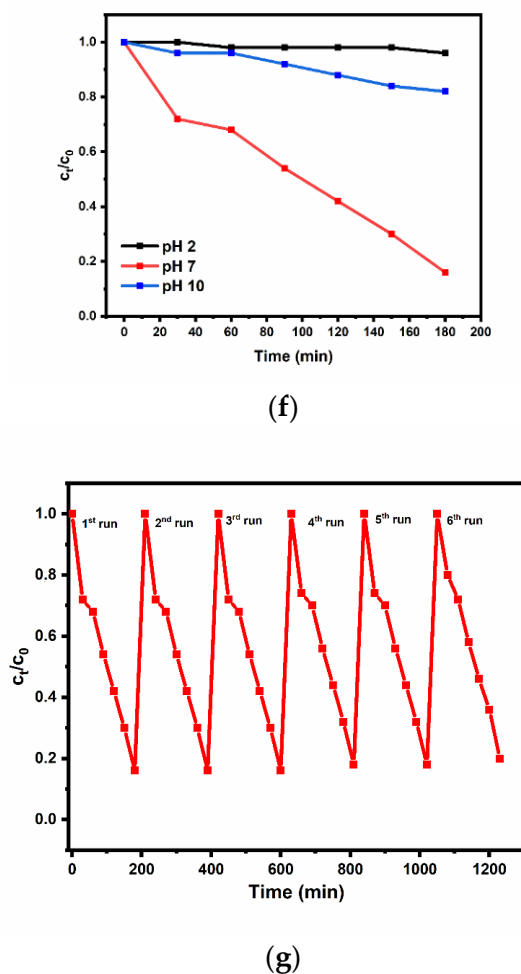


Figure 4. (a) UV-Vis spectra of PEC degradation of paracetamol; (b) normalised concentration decay versus time plot for photocatalytic, electrocatalytic and photoelectrocatalytic degradation of paracetamol on of $\text{Bi}_2\text{WO}_6\text{-CNP-TiO}_2$ NTA electrode and (c) corresponding kinetics plots; (d) normalised concentration decay versus time plot for PEC degradation of Paracetamol on of $\text{Bi}_2\text{WO}_6\text{-CNP-TiO}_2$ NTA electrode. (e) Effects of current density and (f) pH on the degradation of paracetamol. (g) Reusability cycle experiments for the degradation of paracetamol on of $\text{Bi}_2\text{WO}_6\text{-CNP-TiO}_2$ NTA electrode.

The kinetic of paracetamol degradation for each process was investigated using Langmuir-Hinshelwood pseudo first order kinetic equation. The degradation rate constant using the z-scheme electrode for PEC, EC and PC were 0.00987 min^{-1} , 0.00352 min^{-1} and 0.00243 min^{-1} , respectively. This reveals that the degradation of paracetamol was faster when the z-scheme electrode was applied in photoelectrocatalysis, as shown in Figure 3c. Figure 4d depicts the effect of different amounts of CNP to Bi_2WO_6 on the fabrication of $\text{Bi}_2\text{WO}_6\text{-CNP-TiO}_2$ NTA photoanode. The results clearly indicate that above 10% wt of CNP, the degradation of paracetamol is suppressed, therefore it is important to keep the amount of CNP minimal for maximum PEC degradation efficiency. Since 10% gave the highest degradation efficiency, it was used for the preparation of the $\text{Bi}_2\text{WO}_6\text{-CNP-TiO}_2$ NTA electrode. The effect of parameters such as current density and pH were investigated as shown in Figure 4e,f, respectively. The degradation efficiency increased with an increase in current density ranging from 5 mA cm^{-2} to 10 mA cm^{-2} (Figure 4e). This shows that the production of hydroxyl radicals depends on the applied current density. However, current densities should be kept at the optimum to prevent electrode leaching and the production of scavenging radicals. A high current density gives rise to oxygen evolution,

which prevents the generation of hydroxyl radicals, which can suppress the degradation efficiency [12].

The surface charge of the catalyst, drug molecule, radicals and solvent molecules affects the photoelectrocatalytic reaction process under different pH conditions (Sharma et al., 2020). According to previous studies, the point of zero charge for Bi_2WO_6 and TiO_2 are 5.5 and 6.2, respectively (Sharma et al., 2020). Therefore, at an acidic pH value, the surface of the catalyst becomes positively charged. As presented in Figure 3f under acidic conditions (pH 2), a degradation efficiency of 4% was obtained. It was also reported that paracetamol is in its protonated form under acidic conditions [28], hence the result obtained could be due to the repulsion between the surface of the catalyst and the drug molecule. At pH 10, a degradation efficiency of 18% was obtained. In alkaline conditions, more hydroxyl radicals are formed; however, paracetamol is in its deprotonated form [28], thus the repulsion between the negatively charged solution and the drug molecule could minimize the degradation efficiency. A maximum degradation efficiency of 84% was obtained at pH 7 where paracetamol is in its neutral form.

An ideal photoanode is projected to be stable and reusable. The stability and reusability of the prepared of Bi_2WO_6 -CNP- TiO_2 NTA photoanode was investigated by using the same electrode six times; after each cycle the electrode was gently rinsed with deionized water and air dried. As shown in Figure 4g, the degradation efficiency decreased by only 2% after the sixth cycle. This suggests a good stability and reusability of photoanode for PEC degradation.

3.5. Plausible Mechanism for Paracetamol Degradation

The position of the conduction band and valence band of Bi_2WO_6 and TiO_2 was determined using the calculations from UV-DRS studies and the following equations:

$$E_{VB} = X_e - E_e + 0.5E_g \quad (1)$$

$$E_{CB} = E_{VB} - E_g \quad (2)$$

where E_{CB} , E_{VB} , X_e , E_e and E_g are the conduction band of the semiconductor, valence band of the semiconductor, the absolute electronegativity of the semiconductor, energy of free electrons on the hydrogen scale (4.5 eV) and the band gap energy of the semiconductor, respectively. Therefore, E_{VB} and E_{CB} of Bi_2WO_6 are 3.05 eV and 0.35 eV, while E_{VB} and E_{CB} for TiO_2 are 3.285 eV and 0.12 eV, respectively. Based on the approximate bandgap energy values of Bi_2WO_6 and TiO_2 NTA a multiple charge transfer mechanism is followed for the degradation of paracetamol. When the prepared Bi_2WO_6 -CNP- TiO_2 NTA is irradiated by solar light, Bi_2WO_6 and TiO_2 NTA undergo excitation, where electrons migrate from the VB to the CB, leaving positively charged holes on the VB and electron (negative charge) on the CB. However, the electrons on the CB of Bi_2WO_6 migrate through the CNP to the holes on the VB of TiO_2 NTA. The electron transportation that occurs through the carbon nanoparticles enhances the separation of electrons and holes of CB of TiO_2 NTA and VB of Bi_2WO_6 , respectively. The separated electrons on the CB of TiO_2 NTA and the separated holes on the VB of Bi_2WO_6 make TiO_2 NTA electron-rich and Bi_2WO_6 hole-rich. The carbon nanoparticles on the surface of Bi_2WO_6 act as a charge transfer bridge, where electrons from Bi_2WO_6 migrate to holes in TiO_2 NTA. The increased number of electrons on TiO_2 NTA react with adsorbed O_2 to form superoxide radicals. The holes in the VB of Bi_2WO_6 can oxidize H_2O to form hydroxyl radicals, which also participates in the degradation of paracetamol.

The role of the active species for photoelectrocatalytic degradation of paracetamol was investigated by conducting a radical suppressing experiment (Figure 5). The holes, hydroxyl radical and superoxides were suppressed using ethylenediaminetetraacetate (EDTA), t-butanol and p-benzoquinone, respectively. When EDTA was added to the solution, the degradation efficiency dropped significantly to 8%. On the other hand, when t-butanol and p-benzoquinone were added in the solution the degradation efficiency

was 34 and 64%, respectively. The results indicate that the hole and hydroxyl radicals play a major role in the degradation of paracetamol, while superoxides play a minor role. The photoelectrocatalytic degradation of paracetamol can be projected to follow Equations (3)–(7).

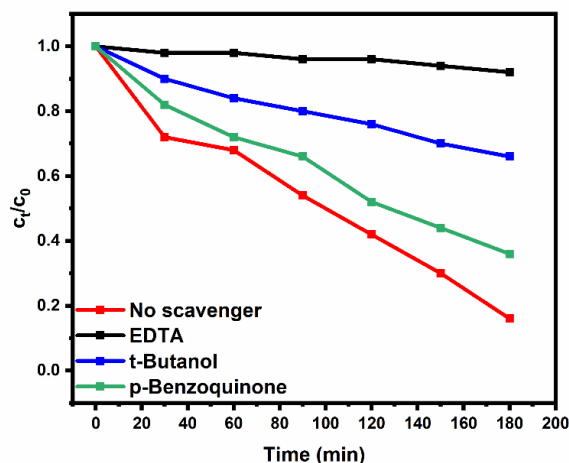
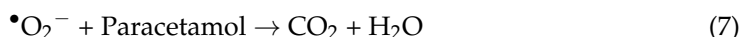
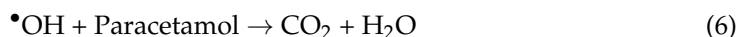
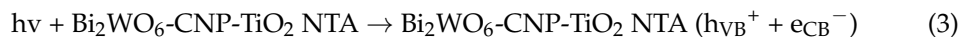


Figure 5. Scavenger studies of the photoelectrocatalytic degradation of Paracetamol on $\text{Bi}_2\text{WO}_6\text{-CNP-TiO}_2$ NTA.

4. Conclusions

A visible light driven ternary z-scheme $\text{Bi}_2\text{WO}_6\text{-CNP-TiO}_2$ NTA heterojunction photoanode was successfully prepared for photoelectrocatalytic application of the water treatment process. FESEM images showed that the catalyst was formed by an agglomerated rod-like structure of $\text{Bi}_2\text{WO}_6\text{-CNP}$ and highly ordered TiO_2 NTA, while EDS mapping supported the formation of the catalyst by showing all the elements present. The formation of the z-scheme heterojunction enhanced the visible light activity of the semiconductor heterojunctions. The formation of the z-scheme also improved the photocurrent response to about 4.6 times higher and charge carrier separation. When the z-scheme heterojunction photoanode was applied for PEC degradation of paracetamol, a degradation efficiency of 84% was obtained within 180 min. Scavenger studies revealed that the holes played a major role in the degradation process. The electrode showed excellent stability and reusability, hence the reported photoanode shows great potential for the photoelectrochemical application of organic pollutants.

Author Contributions: Conceptualization, N.M. and O.A.A.; methodology, N.M., L.M.C. and O.A.A.; validation, N.M. and O.A.A.; formal analysis, N.M.; investigation, N.M.; resources, O.A.A.; writing—original draft preparation, N.M.; writing—review and editing, L.M.C., O.A.A., C.M., O.V.N., B.A.K.; supervision, L.M.C. and O.A.A.; project administration, L.M.C.; funding acquisition, O.A.A. All authors have read and agreed to the published version of the manuscript.

Funding: This research was funded by National Research Foundation, South Africa, grant number 118546 and Centre for Nanomaterials Science Research, University of Johannesburg, South Africa.

Institutional Review Board Statement: Not applicable.

Informed Consent Statement: Not applicable.

Data Availability Statement: Not applicable.

Conflicts of Interest: The authors declare no conflict of interest.

References

1. Olvera-Rodríguez, I.; Hernández, R.; Medel, A.; Guzmán, C.; Escobar-Alarcón, L.; Brillas, E.; Sirés, I.; Esquivel, K. TiO₂ /Au/ TiO₂ Multilayer Thin-Film Photoanodes Synthesized by Pulsed Laser Deposition for Photoelectrochemical Degradation of Organic Pollutants. *Sep. Purif. Technol.* **2019**, *224*, 189–198. [[CrossRef](#)]
2. Högestätt, E.D.; Jönsson, B.A.G.; Ermund, A.; Andersson, D.A.; Björk, H.; Alexander, J.P.; Cravatt, B.F.; Basbaum, A.I.; Zygmunt, P.M. Conversion of Acetaminophen to the Bioactive N-Acylphenolamine AM404 via Fatty Acid Amide Hydrolase-Dependent Arachidonic Acid Conjugation in the Nervous System. *J. Biol. Chem.* **2005**, *280*, 31405–31412. [[CrossRef](#)] [[PubMed](#)]
3. López Zavala, M.Á.; Jaber Lara, C.R. Degradation of Paracetamol and Its Oxidation Products in Surface Water by Electrochemical Oxidation. *Environ. Eng. Sci.* **2018**, *35*, 1248–1254. [[CrossRef](#)] [[PubMed](#)]
4. Dalgic, G.; Turkdogan, F.I.; Yetilmesoy, K.; Kocak, E. Treatment of Real Paracetamol. *Chem. Ind. Chem. Eng. Q* **2017**, *23*, 177–186. [[CrossRef](#)]
5. Fatima, S.; Asif, N.; Ahmad, R.; Fatma, T. Toxicity of NSAID Drug (Paracetamol) to Nontarget Organism—Nostoc Muscorum. *Environ. Sci. Pollut. Res.* **2020**, *27*, 35208–35216. [[CrossRef](#)]
6. Macías-García, A.; García-Sanz-Calcedo, J.; Carrasco-Amador, J.P.; Segura-Cruz, R. Adsorption of Paracetamol in Hospital Wastewater through Activated Carbon Filters. *Sustainability* **2019**, *11*, 2672. [[CrossRef](#)]
7. Lozano-Morales, S.A.; Morales, G.; López Zavala, M.Á.; Arce-Sarria, A.; Machuca-Martínez, F. Photocatalytic Treatment of Paracetamol Using TiO₂ Nanotubes: Effect of PH. *Processes* **2019**, *7*, 319. [[CrossRef](#)]
8. Audino, F.; Santamaria, J.M.T.; Del Valle Mendoza, L.J.; Graells, M.; Pérez-Moya, M. Removal of Paracetamol Using Effective Advanced Oxidation Processes. *Int. J. Environ. Res. Public Health* **2019**, *16*, 505. [[CrossRef](#)]
9. Ghanbari, F.; Giannakis, S.; Lin, K.Y.A.; Wu, J.; Madihi-Bidgoli, S. Acetaminophen Degradation by a Synergistic Peracetic Acid/UVC-LED/Fe(II) Advanced Oxidation Process: Kinetic Assessment, Process Feasibility and Mechanistic Considerations. *Chemosphere* **2021**, *263*, 128119. [[CrossRef](#)]
10. Arotiba, O.A.; Orimolade, B.O.; Koiki, B.A. Visible Light-Driven Photoelectrocatalytic Semiconductor Heterojunction Anodes for Water Treatment Applications. *Curr. Opin. Electrochem.* **2020**, *22*, 25–34. [[CrossRef](#)]
11. Orimolade, B.O.; Arotiba, O.A. Towards Visible Light Driven Photoelectrocatalysis for Water Treatment: Application of a FTO/BiVO₄/Ag₂S Heterojunction Anode for the Removal of Emerging Pharmaceutical Pollutants. *Sci. Rep.* **2020**, *10*, 5348. [[CrossRef](#)] [[PubMed](#)]
12. Orimolade, B.O.; Koiki, B.A.; Zwane, B.N.; Peleyeju, G.M.; Mabuba, N.; Arotiba, O.A. Interrogating Solar Photoelectrocatalysis on an Exfoliated Graphite-BiVO₄/ZnO Composite Electrode towards Water Treatment. *RSC Adv.* **2019**, *9*, 16586–16595. [[CrossRef](#)] [[PubMed](#)]
13. Nada, A.A.; Orimolade, B.O.; El-Maghrabi, H.H.; Koiki, B.A.; Rivallin, M.; Bekheet, M.F.; Viter, R.; Damberga, D.; Lesage, G.; Iatsunskyi, I.; et al. Photoelectrocatalysis of Paracetamol on Pd-ZnO/N-Doped Carbon Nanofibers Electrode. *Appl. Mater. Today* **2021**, *24*, 101129. [[CrossRef](#)]
14. Sharma, S.; Ibhaddon, A.O.; Francesconi, M.G.; Mehta, S.K.; Elumalai, S.; Kansal, S.K.; Umar, A.; Baskoutas, S. Bi₂WO₆/C-Dots /TiO₂: A Novel Z-Scheme Photocatalyst for the Degradation of Fluoroquinolone Levofloxacin from Aqueous Medium. *Nanomaterials* **2020**, *10*, 910. [[CrossRef](#)]
15. Hu, K.; Chen, C.; Zhu, Y.; Zeng, G.; Huang, B.; Chen, W.; Liu, S.; Lei, C.; Li, B.; Yang, Y. Ternary Z-Scheme Heterojunction of Bi₂WO₆ with Reduced Graphene Oxide (RGO) and Meso-Tetra (4-Carboxyphenyl) Porphyrin (TCPP) for Enhanced Visible-Light Photocatalysis. *J. Colloid Interface Sci.* **2019**, *540*, 115–125. [[CrossRef](#)]
16. Adhikari, S.; Selvaraj, S.; Kim, D.H. Construction of Heterojunction Photoelectrode via Atomic Layer Deposition of Fe₂O₃ on Bi₂WO₆ for Highly Efficient Photoelectrochemical Sensing and Degradation of Tetracycline. *Appl. Catal. B Environ.* **2019**, *244*, 11–24. [[CrossRef](#)]
17. Syed, N.; Huang, J.; Feng, Y.; Wang, X.; Cao, L. Carbon-Based Nanomaterials via Heterojunction Serving as Photocatalyst. *Front. Chem.* **2019**, *7*, 713. [[CrossRef](#)]
18. Rana, A.; Kumar, A.; Sharma, G.; Naushad, M.; Bathula, C.; Stadler, F.J. Pharmaceutical Pollutant as Sacrificial Agent for Sustainable Synergistic Water Treatment and Hydrogen Production via Novel Z- Scheme Bi₂O₉I₃/B₄C Heterojunction Photocatalysts. *J. Mol. Liq.* **2021**, *343*, 117652. [[CrossRef](#)]
19. Chaplin, B.P. Critical Review of Electrochemical Advanced Oxidation Processes for Water Treatment Applications. *Environ. Sci. Process. Impacts* **2014**, *16*, 1182–1203. [[CrossRef](#)]
20. Velepini, T.; Prabakaran, E.; Pillay, K. Recent Developments in the Use of Metal Oxides for Photocatalytic Degradation of Pharmaceutical Pollutants in Water—A Review. *Mater. Today Chem.* **2021**, *19*, 100380. [[CrossRef](#)]

21. Borràs-Ferrís, J.; Sánchez-Tovar, R.; Blasco-Tamarit, E.; Muñoz-Portero, M.J.; Fernández-Domene, R.M.; García-Antón, J. TiO₂ Nanostructures for Photoelectrocatalytic Degradation of Acetaminophen. *Nanomaterials* **2019**, *9*, 583. [[CrossRef](#)] [[PubMed](#)]
22. Koiki, B.A.; Orimolade, B.O.; Zwane, B.N.; Nkosi, D.; Mabuba, N.; Arotiba, O.A. Cu₂O on Anodised TiO₂ Nanotube Arrays: A Heterojunction Photoanode for Visible Light Assisted Electrochemical Degradation of Pharmaceuticals in Water. *Electrochim. Acta* **2020**, *340*, 135944. [[CrossRef](#)]
23. Cheng, T.; Gao, H.; Liu, G.; Pu, Z.; Wang, S.; Yi, Z.; Yang, H. Preparation of core-shell heterojunction photocatalysts by coating CdS nanoparticles onto Bi₄Ti₃O₁₂ hierarchical microspheres and their photocatalytic removal of organic pollutants and Cr (VI) ions. *Colloids Surf. A Physicochem. Eng. Asp.* **2022**, *633*, 127918. [[CrossRef](#)]
24. Umukoro, E.H.; Peleyeju, M.G.; Idris, A.O.; Ngila, J.C.; Mabuba, N.; Rhyman, L.; Ramasami, P.; Arotiba, O.A. Photoelectrocatalytic application of palladium decorated zinc oxide-expanded graphite electrode for the removal of 4-nitrophenol: Experimental and computational studies. *RSC Adv.* **2018**, *8*, 10255–10266. [[CrossRef](#)] [[PubMed](#)]
25. Khedr, T.M.; Wang, K.; Kowalski, D.; El-Sheikh, S.M.; Abdeldayem, H.M.; Ohtani, B.; Kowalska, E. Bi₂WO₆-based Z-scheme photocatalysts: Principles, mechanisms and photocatalytic applications. *J. Environ. Chem. Eng.* **2022**, *10*, 107838. [[CrossRef](#)]
26. Peleyeju, M.G.; Arotiba, O.A. Recent trend in visible-light photoelectrocatalytic systems for degradation of organic contaminants in water/wastewater. *Environ. Sci. Water Res. Technol.* **2018**, *4*, 1389–1411. [[CrossRef](#)]
27. Tshwenya, L.; Arotiba, O.A. Ethylenediamine Functionalized Carbon Nanoparticles: Synthesis, Characterization, and Evaluation for Cadmium Removal from Water. *RSC Adv.* **2017**, *7*, 34226–34235. [[CrossRef](#)]
28. Bernal, V.; Erto, A.; Giraldo, L.; Moreno-Piraján, J.C. Effect of Solution PH on the Adsorption of Paracetamol on Chemically Modified Activated Carbons. *Molecules* **2017**, *22*, 1032. [[CrossRef](#)]